

The optimal schedule for pulsar timing array observations

K. J. Lee^{1,2*}, C. G. Bassa², G. H. Janssen², R. Karuppusamy^{1,2},
M. Kramer^{1,2}, R. Smits^{2,3} and B. W. Stappers²

¹Max-Planck-Institut für Radioastronomie, Auf dem Hügel 69, D-53121 Bonn, Germany

²Jodrell Bank Centre for Astrophysics, University of Manchester, Manchester M13 9PL, UK

³Stichting ASTRON, Postbus 2, 7990 AA Dwingeloo, The Netherlands

3 June 2021

ABSTRACT

In order to maximize the sensitivity of pulsar timing arrays to a stochastic gravitational wave background, we present computational techniques to optimize observing schedules. The techniques are applicable to both single and multi-telescope experiments. The observing schedule is optimized for each telescope by adjusting the observing time allocated to each pulsar while keeping the total amount of observing time constant. The optimized schedule depends on the timing noise characteristics of each individual pulsar as well as the performance of instrumentation. Several examples are given to illustrate the effects of different types of noise. A method to select the most suitable pulsars to be included in a pulsar timing array project is also presented.

Key words: pulsar: general — gravitational wave

1 INTRODUCTION

Millisecond pulsars (MSPs) are stable celestial clocks, so that the timing residuals, the differences between the observed and the predicted time of arrival (TOA) of their pulses, are usually minute compared to the total length of the data span. A stochastic gravitational wave (GW) background leaves angular dependent correlations in the timing residuals of widely separated pulsars (for general relativity see Hellings & Downs 1983, for alternative gravity theories see Lee et al. 2008, 2010), i.e. the correlation coefficient between timing residuals of a pulsar pair is a function of the angular distance between the two pulsars. Such a spatial correlation in pulsar timing signals makes it possible to directly detect GW using pulsar timing arrays (PTAs; Hellings & Downs 1983; Foster & Backer 1990). Previous analyses (Jenet et al. 2005) have calculated PTA sensitivity to a stochastic GW background generated by super massive blackhole (SMBH) binaries at cosmological distances (Jaffe & Backer 2003; Sesana et al. 2004). They have shown that a positive detection of the GW background is feasible, if one uses state of the art pulsar timing technologies. Such encouraging results triggered consequent observational efforts.

At present, several groups are trying to detect GWs using PTAs: i) the European Pulsar Timing Array (EPTA; Stappers et al. 2006; Lazaridis 2010; Ferdman et al. 2010;

van Haasteren et al. 2011) with a sub-project, the Large European Array for Pulsars (LEAP, Kramer & Stappers 2010; Ferdman et al. 2010), combining data from the Lovell telescope, the Westerbork Synthesis Radio Telescope, the Effelsberg 100-m Radio Telescope, the Nançay Decimetric Radio Telescope, and the Sardinia Radio Telescope¹, ii) the Parkes Pulsar Timing Array (PPTA; Manchester 2008; Hobbs et al. 2009; Verbiest et al. 2010) using observations with the Parkes radio telescope augmented by public domain observations from the Arecibo Observatory, iii) the North-American Nanohertz Observatory for Gravitational waves (NANOGrav, Jenet et al. 2009) using data from the Green Bank Telescope and the Arecibo Observatory, iv) Kalyazin Radio Astronomical Observatory timing (Rodin 2011). Besides these on-going projects, international cooperative efforts, e.g. the International Pulsar Timing Array (IPTA, Hobbs & et al. 2010) or future telescopes with better sensitivity, e.g. the Five-hundred-meter Aperture Spherical Radio Telescope (FAST, Nan et al. 2006; Smits et al. 2009) and the Square Kilometre Array (SKA, Kramer & Stappers 2010; Smits et al. 2009), are planned to join the PTA projects to increase the chances of detecting GWs.

Operational questions arise naturally from such PTA campaigns, e.g. how should the observing schedule be arranged to maximize our opportunity to detect the GW sig-

* Email: kjlee@mpifr-bonn.mpg.de

¹ The Sardinia Radio telescope is in the commissioning phase at the time of writing this paper.

nal? How much will we benefit from such optimization? In this paper, we try to answer these questions. The paper is organized as follows: In Section 2, we extend the formalism of Jenet et al. (2005) to calculate the GW detection significance as a function of observing schedules, i.e. the telescope time allocation to each pulsar. Then we describe the technique to maximize the GW detection significance in Section 3. Frameworks of the optimization problem are described in Section 3.1, and the algorithm to optimize a single and multiple telescope array are given in Section 3.2 and Section 3.3 respectively. The results are presented in Section 4 and we discuss related issues in Section 5.

2 ANALYTICAL CALCULATION FOR GW DETECTION SIGNIFICANCE

In this section, we calculate the statistical significance S for detecting the stochastic GW background using PTAs. We consider TOAs from multiple pulsars, where each set may be collected from different telescopes or data acquisition systems. To detect the GW background, one correlates the TOAs between pulsar pairs and checks if the GW-induced correlation is significant. Jenet et al. (2005) have calculated the GW detection significance for the case, where the noise in TOAs is of a white spectra with equal root-mean-square (RMS) level for all pulsars. To investigate the optimal observing schedule, we have to generalize the calculation, such that we can explicitly check the dependence of the GW detection significance on the noise properties of each individual pulsar.

Under the influence of a stochastic gravitational wave background, the pulsar timing residual R from a standard pulsar timing pipeline contains two components, the GW-induced signal s and noise from other contributions n . In this section, we determine the statistical properties of s and n first, and then calculate the GW detection significance.

2.1 Statistics for GW-induced pulsar timing signal

The spectrum of the stochastic GW background is usually assumed to be a power-law, in which the characteristic strain (h_c) of the GW background is $h_c = A_0(f/f_0)^\alpha$. Here, A_0 is the dimensionless amplitude for the background at $f_0 = 1 \text{ yr}^{-1}$, and α is the spectral index. Under the influence of such a GW background, the power spectrum $S_s(f)$ of the GW-induced pulsar timing residual s is (Jenet et al. 2005)

$$S_s(f) = \frac{A_0^2 f^{2\alpha-3}}{12\pi^2 f_0^{2\alpha}}. \quad (1)$$

GWs perturb the space-time metric at the Earth. This introduces a correlation in the timing signal of two pulsars. The correlation coefficient $H(\theta)$ between the GW-induced signals of two pulsars with an angular separation of θ is called the Hellings and Downs function (Hellings & Downs 1983) given as

$$H(\theta) = \begin{cases} \frac{3+\cos\theta}{8} - \frac{3(\cos\theta-1)}{2} \ln \left[\sin \left(\frac{\theta}{2} \right) \right], & \text{if } \theta \neq 0, \\ 1, & \text{if } \theta = 0. \end{cases} \quad (2)$$

The spectral properties, equation (1), together with the spatial correlation, equation (2), fully characterize the statistical properties of the GW-induced signals.

For an isotropic GW background, the correlations between the GW-induced signals are

$$\langle {}^i s_k {}^j s_{k'} \rangle = \sigma_g^2 H({}^{ij}\theta) \gamma_{kk'}. \quad (3)$$

Here, we follow the notation that the subscript on the right is the index of sampling and the superscript on the left is the index for the pulsar. For example, we denote the k -th measurement of a timing residual of the i -th pulsar as ${}^i R_k$, the GW-induced signal as ${}^i s_k$ and other noise contributions as ${}^i n_k$. σ_g is the RMS level for the GW-induced signal, ${}^{ij}\theta$ is the angular distance between the i -th and j -th pulsar, and $\gamma_{kk'}$ is the temporal correlation coefficient between the k -th and k' -th sampling. σ_g and $\gamma_{kk'}$ are numerically calculated from the GW spectrum as shown in Appendix A.

2.2 Statistics of noise components from other contributions

A purely theoretical modeling of the noise part n is complex, because it (Foster & Backer 1990; Shannon & Cordes 2010; Cordes & Shannon 2010) depends on the properties of each individual pulsar, the instrumentation, and radio frequency interference. We therefore model the noise phenomenologically using observational knowledge. In this paper, the noise part of a pulsar timing residual is modeled as a superposition of a white noise component and a red noise component, where the white noise is designated to the measurement uncertainty on the TOA due to radiometer noise and pulse jitter noise (Liu et al. 2012). Timing residuals of several millisecond pulsars show clear evidence of temporally correlated noise, although its origin is not yet clear (Verbiest et al. 2009). The red noise components are used to empirically model such effects. We further assume that the noise components are not correlated between any two different pulsars².

For each pulsar, three parameters are used to characterize the noise spectrum. These parameters are the RMS level of the white noise ${}^i \sigma_w$, the RMS level for red noise ${}^i \sigma_r$, and the spectral index for the red noise ${}^i \beta$. The white noise spectrum is

$${}^i S_w(f) = \frac{{}^i \sigma_w}{\widetilde{\sigma}_w}, \quad (4)$$

and the red noise spectrum is

$${}^i S_r(f) = \frac{{}^i \sigma_r f^{i\beta}}{\widetilde{\sigma}_r}, \quad (5)$$

where the $\widetilde{\sigma}_w$ and $\widetilde{\sigma}_r$ are for normalization. From the spectrum, one can derive the correlation between noise components

$$\langle {}^i n_k {}^j n_{k'} \rangle = \left({}^i \sigma_w^2 \delta_{kk'} + {}^i \sigma_r^2 g_{kk'} \right) \delta_{ij}. \quad (6)$$

Following our conventions, ${}^i n_k$ is the noise for the k -th sampling of the i -th pulsar. The δ_{ij} is the 'Kronecker delta' symbol, i.e. $\delta_{ij} = 1$, if $i = j$, otherwise $\delta_{ij} = 0$. The parameters $\widetilde{\sigma}_w$, $\widetilde{\sigma}_r$, and correlation coefficients $g_{kk'}$ are calculated using a numerical simulation shown in Appendix A.

² The correlated noise such as clock noise is discussed in Section 5 and Appendix E

2.3 GW background detection significance

Following Jenet et al. (2005), we calculate the cross power ${}^{ij}c$ between timing residuals and then compare it with the predicted correlation coefficient $H(\theta)$ to check whether the GW signal is significant. The cross power ${}^{ij}c$ is

$${}^{ij}c = \frac{1}{m} \sum_{k=1}^m {}^iR_k {}^jR_k, \quad (7)$$

where ${}^iR_k, {}^jR_k$ are the timing residuals of the i -th and the j -th pulsars for the k -th timing session, m is the number of data points for a given pulsar. It is assumed that the data from different pulsars overlap with each other and the number of data points is identical for all the pulsars, similar to the discussion in Yardley et al. (2011). These assumptions are good approximations in calculating the GW detection sensitivity. In the case where the TOAs are mis-aligned or the number of data points is not identical, one can combine data points so that the number of data points are identical. This operation retains most of the GW detection sensitivity due to: i) The RMS error reduces when data is combined, and such a reduction in RMS error compensates the reduction in the number of data points. ii) The spectrum of the GW induced timing signal is steep, thus most of the GW induced signal is in the low frequency components, which are preserved during the combining operation.

The comparison between the ${}^{ij}c$ and the Hellings-Downs function is carried out by doing another correlation, which gives the GW detection significance S as

$$S = \sqrt{M} \frac{\sum_{i-j \text{ pairs}} ({}^{ij}c - \bar{c})(H({}^{ij}\theta) - \bar{H})}{\sqrt{\sum_{i-j \text{ pairs}} ({}^{ij}c - \bar{c})^2 \sum_{i-j \text{ pairs}} (H({}^{ij}\theta) - \bar{H})^2}}, \quad (8)$$

where the summation $\sum_{i-j \text{ pairs}}$ sums over all independent pulsar pairs except the case where $i = j$, i.e.

$$\sum_{i-j \text{ pairs}} \equiv \sum_{i=1}^N \sum_{j=1}^{i-1}, \quad (9)$$

and

$$\bar{c} = \frac{1}{M} \sum_{i-j \text{ pairs}} {}^{ij}c, \quad (10)$$

$$\bar{H} = \frac{1}{M} \sum_{i-j \text{ pairs}} H({}^{ij}\theta). \quad (11)$$

Given N pulsars, the sum $M = \sum_{i-j \text{ pairs}} 1 = N(N-1)/2$ is the number of independent pulsar pairs. To evaluate the quality of the detector, we need the expectation for the detection significance $\langle S \rangle$, which is

$$\langle S \rangle \simeq \frac{\sum_{i-j \text{ pairs}} \langle ({}^{ij}c - \bar{c})(H({}^{ij}\theta) - \bar{H}) \rangle}{\sqrt{M \Sigma_c \Sigma_H}}, \quad (12)$$

where

$$\Sigma_H = \sqrt{\frac{1}{M} \sum_{i-j \text{ pairs}} [H({}^{ij}\theta) - \bar{H}]^2}, \quad (13)$$

$$\Sigma_c = \sqrt{\left\langle \frac{1}{M} \sum_{i-j \text{ pairs}} [c({}^{ij}\theta) - \bar{c}]^2 \right\rangle}, \quad (14)$$

and the $\langle \cdot \rangle$ denotes the ensemble average. As we show in

Appendix B, the expected GW detection significance is

$$\langle S \rangle \simeq \sqrt{M} \left[1 + \frac{\sum_{i-j \text{ pairs}} ({}^{ij}A + {}^{ij}B)}{M \Sigma_H^2} \right]^{-\frac{1}{2}}, \quad (15)$$

where

$${}^{ij}A = \frac{1}{m^2} \sum_{kk'} \left[\left(1 + H({}^{ij}\theta) \right) \gamma_{kk'}^2 + \left({}^i\eta_{r,kk'} + {}^j\eta_{r,kk'} \right) \gamma_{kk'} + {}^i\eta_{r,kk'} {}^j\eta_{r,kk'} \right], \quad (16)$$

$${}^{ij}B = \frac{1}{m} \left({}^i\eta_w + {}^j\eta_w + {}^i\eta_w {}^j\eta_w + {}^i\eta_r {}^j\eta_w + {}^j\eta_r {}^i\eta_w \right), \quad (17)$$

and η denotes the ratio between the power of noise components and the power of the GW-induced signal, which are

$${}^i\eta_{r,kk'} = \frac{{}^i\sigma_r^2 g_{kk'}}{\sigma_g^2} \quad (18)$$

$${}^i\eta_r = \frac{{}^i\sigma_r^2}{\sigma_g^2} \quad (19)$$

$${}^i\eta_w = \frac{{}^i\sigma_w^2}{\sigma_g^2}. \quad (20)$$

If the noise level ${}^i\sigma_n$ is identical for all pulsars and there is no red noise component (${}^i\sigma_w = {}^j\sigma_w$ and ${}^i\sigma_r = 0$ for all the $i, j = 1 \dots N$), equation (15) reduces to the result found by Jenet et al. (2005) and Verbiest et al. (2009).

The ${}^{ij}A$ terms are independent of telescope integration time, because they only contain the RMS level of the GW-induced signal and the red noise, both of which are independent of telescope integration time. The observing schedule, the plan of allocating telescope time to each pulsar, only changes terms of ${}^{ij}B$, which depend on the ratio between signal and noise amplitude. By optimizing the observing schedule, we can reduce the summation of ${}^{ij}B$, such that the GW detection significance is maximized. We present the technique to maximize the GW detection significance in the next section.

3 OPTIMIZATION OF THE GW DETECTION SIGNIFICANCE UNDER OBSERVING CONSTRAINTS

Pulsar timing observations are usually conducted as a series of successive observing sessions. In each session, multiple pulsars are observed using either one or multiple telescopes. There are basically two ways to use multiple telescopes. The simple way is to use each telescope independently, combine the TOA data from each telescope, remove the time jumps between each data set, and form a single TOA data set (Janssen et al. 2008). The other way, as in the LEAP project, is to use telescopes simultaneously to form a phased array and then calculate the TOAs from the phased-array data. Due to such different methods of using multiple telescopes, the optimization techniques differ from one another. We answer the following questions in this section: i) What are the variables to optimize? ii) What are the constraints on the optimization? iii) How do we perform the optimization?

3.1 The objective, variables, and constraints of the optimization

Given a fixed amount of telescope time, we can adjust the amount of observing time allocated to each pulsar. Increasing the observing time for one pulsar will reduce its timing measurement error, but will increase the timing error for other pulsars. Naturally, for the purpose of detecting GWs, the optimization objective is to maximize the expected GW detection significance $\langle S \rangle$, while the constraint is the total amount of telescope time for the project.

Generally, for a timing project using N_{tel} telescopes to observe N pulsars, we need $2N_{\text{tel}} + 3N$ input parameters to characterize the whole timing project. $2N_{\text{tel}}$ parameters are used to characterize N_{tel} telescopes, where each telescope is quantified by the *gain* (\mathcal{G}) and the *total available telescope time* (τ). $3N$ parameters are used to characterize the timing behavior of N pulsars. The red noise level σ_r and spectral index β are assumed to be pulsar intrinsic. The observed white noise RMS levels σ_w depend on telescope gain, telescope time allocation to the pulsar and other parameters intrinsic to the pulsar (e.g. flux, pulse width, and so on).

For single telescope cases, we can encapsulate the dependence of the white noise level on the schedule into the normalized white noise level σ_0 and pulse jitter noise level σ_J (Foster & Backer 1990; Shannon & Cordes 2010; Cordes & Shannon 2010)

$$i\sigma_w = \left(i\sigma_0^2 \mathcal{G}^{-2} + i\sigma_J^2 \right)^{1/2} \left(\frac{i\tau}{1\text{hr}} \right)^{-1/2}, \quad (21)$$

where $i\sigma_w$ is the measured RMS level for the white noise component of the i -th pulsar, $i\tau$ is the telescope time being used for the i -th pulsar per observing session, and \mathcal{G} is the telescope gain. The normalized noise level $i\sigma_0$ and the $i\sigma_J$ are used to characterize the radiometer noise and the pulse jitter noise of the pulsar. On the one hand, if there is no pulse jitter noise, σ_0 will be the observed RMS level of the white noise for a 1 hour observation using a telescope with unit gain $\mathcal{G} = 1^3$. On the other hand, if we have a telescope with infinite gain, the pulsar timing accuracy will be limited by the pulse jitter, and σ_J will be the observed RMS level of white noise for a 1 hour observation. If phased array observations are performed using multiple telescopes (as done in the LEAP project), the situation is identical to the case of a single telescope, and we use the effective gain for the array to determine the RMS level of noise.

For multiple incoherent telescopes, the gain of N_{tel} telescopes can be summarized by a vector \mathcal{G}_ν , where $\nu = 1 \dots N_{\text{tel}}$ and the ν -th component \mathcal{G}_ν is the gain for the ν -th telescope. In a similar fashion, the available telescope time of each telescope is summarized by the vector τ_ν . The definition of the observing schedule becomes more complex, since we need to specify the observation time for each pulsar using each telescope. Furthermore, the schedule should also include information on the telescope availability, e.g. certain pulsars may not be visible to some telescopes due to geographical reasons. In this paper, we use the *resource allocation matrix* \mathbf{O} to describe the telescope availability,

³ In this paper, we use a fiducial unit for the gain, thus one can take any telescope as unit 1 and scale other telescopes accordingly.

where the i -th row and ν -th column element iO_ν indicates whether we use the ν -th telescope to observe the i -th pulsar, i.e. $iO_\nu = 1$, if the ν -th telescope observes the i -th pulsar, and $iO_\nu = 0$ otherwise. The telescope time allocation is described by another matrix, the *schedule matrix* \mathbf{P} , where the i -th row ν -th column element iP_ν is the time allocated for the ν -th telescope observing the i -th pulsar.

With the schedule matrix \mathbf{P} , the equivalent RMS level of the white noise in the combined data is

$$i\sigma_w = \left[i\sigma_0^2 \left(\sum_{\nu=1}^{N_{\text{tel}}} \mathcal{G}_\nu^2 iP_\nu iO_\nu \right)^{-1} + i\sigma_J^2 \left(\sum_{\nu=1}^{N_{\text{tel}}} iP_\nu iO_\nu \right)^{-1} \right]^{1/2}. \quad (22)$$

The main reason to introduce the resource allocation matrix iO_ν is to take care of the complexity of telescope availability, and the telescope time can be treated in an identical way independent of the availability.

For a single telescope or a phased array, the optimization constraint is

$$\tau = \sum_{i=1}^N i\tau, \quad (23)$$

i.e. the total telescope time is pre-fixed to be τ . For multiple incoherent telescopes, the above constraint is applied to each telescope individually, i.e. the constraints specify the available observation time τ_ν for each telescope, which gives

$$\tau_\nu = \sum_{i=1}^N iP_\nu iO_\nu. \quad (24)$$

With the observing schedule (i.e. the vector $i\tau$ for a single telescope or the matrix iO_ν and iP_ν for incoherent telescopes), one can use equation (21) and (22) to determine the white noise level, then determine the GW detection significance as explained in Section 2.3. The optimization of the observing schedule means that we choose an appropriate $i\tau$ or iP_ν such that the expected GW-detection significance $\langle S \rangle$ is maximized under the constraint of equation (23) or (24).

From equation (15), the maximization of $\langle S \rangle$ is equivalent to the minimization of the term $\sum_{i-j \text{ pairs}} (i^j A + i^j B)$. Because the terms of $i^j A$ are independent of the telescope time, the maximization of $\langle S \rangle$ by adjusting the observing schedule is thus equivalent to minimizing the objective function \mathcal{L} defined as

$$\mathcal{L} = \sum_{i-j \text{ pairs}} i^j B. \quad (25)$$

3.2 Optimizing a single telescope

Our technique to optimize the single telescope schedule takes two steps. The first step is to convert the constrained optimization problem to a constraint-free version, and the second step is to solve the constraint-free optimization. For comparison, we have also developed an alternative semi-analytical iterative technique in Appendix C.

To remove the constraints, we transform variables $i\tau$ to a new set of variables θ_μ , where μ is $1 \dots N - 1$, and the

transformation is

$$\begin{pmatrix} \theta_1 \\ \theta_2 \\ \theta_3 \\ \dots \\ \theta_{N-2} \\ \theta_{N-1} \end{pmatrix} = \begin{pmatrix} \arccos\left(\frac{\sqrt{1_\tau}}{\sqrt{\tau}}\right) \\ \arccos\left(\frac{\sqrt{2_\tau}}{\sqrt{\tau} \sin \theta_1}\right) \\ \arccos\left(\frac{\sqrt{3_\tau}}{\sqrt{\tau} \sin \theta_1 \sin \theta_2}\right) \\ \dots \\ \arccos\left(\frac{\sqrt{N-2_\tau}}{\sqrt{\tau} \prod_{i=1}^{N-3} \sin \theta_i}\right) \\ \arccos\left(\frac{\sqrt{N-1_\tau}}{\sqrt{\tau} \prod_{i=1}^{N-2} \sin \theta_i}\right) \end{pmatrix}, \quad (26)$$

of which the inverse transformation is

$$\begin{pmatrix} 1_\tau \\ 2_\tau \\ 3_\tau \\ \dots \\ N-1_\tau \\ N_\tau \end{pmatrix} = \tau \begin{pmatrix} \cos^2 \theta_1 \\ \sin^2 \theta_1 \cos^2 \theta_2 \\ \sin^2 \theta_1 \sin^2 \theta_2 \cos^2 \theta_3 \\ \dots \\ \prod_{\mu=1}^{N-2} \sin^2 \theta_\mu \cos^2 \theta_{N-1} \\ \prod_{\mu=1}^{N-1} \sin^2 \theta_\mu \end{pmatrix}. \quad (27)$$

Here it is implicitly assumed that ${}^i\tau \geq 0$, the \prod_i and \prod_μ are the serial products using the index i and μ respectively. Equations (26) and (27) are, in fact, the transformation between a N -dimensional Cartesian coordinate system and its corresponding hyperspherical coordinate system. The constraint in the new spherical coordinate system corresponds to fixing the radius of the hypersphere (fixing τ), and all angular coordinates θ_μ are free variables for which one can specify any value for θ_μ without breaking the constraint, i.e. after the above coordinate transformation, the objective \mathcal{L} becomes a function of a new variable θ_μ , the constraint equation (23) is automatically satisfied for any θ_μ . We can then find the minimum of \mathcal{L} using numerical methods for constraint-free problems. In this paper, the downhill simplex method (Nelder & Mead 1965) is adopted, which has, usually, better global converging behavior than other methods (Kramer et al. 1994). Once the optimal θ_μ are found, we transform them back to ${}^i\tau$ using equation (27), which yields the optimal single telescope schedule. In practical situations, one also needs to add telescope slewing time, observing time for calibration sources and other necessary auxiliary time on top of this telescope time schedule to get the final schedule.

3.3 Optimizing multiple incoherent telescopes

Similarly to section 3.2, the optimal observing schedule for multiple incoherent telescopes is calculated by minimizing \mathcal{L} , although the constraints are slightly more complex here. In this section, we present the optimizing technique and discuss later the relation between the optimization of multiple telescopes and single telescope optimization.

From the multiple telescope constraint equation (24), we can see that the constraints are applied to each telescope individually. Thus, the generalization of the method presented in the previous section is straightforward by applying the transformation equation (26) to each telescope separately. Take telescope 1 as an example. The first column of matrix \mathbf{P} , the ${}^1P_\nu$, is the observing schedule for the first telescope. We can transform those components of ${}^1P_\nu$ indicated by ${}^1O_\nu = 1$ using equation (26) to remove the constraint of the first telescope. Similarly, by applying the transformation to the other columns of matrix \mathbf{P} successively, one

can remove all the constraints. With the new constraint-free variables, we use the down-hill simplex method to find the optimization. We then transform back to ${}^iP_\nu$, which is the optimization schedule.

In the optimization algorithm, we treat the resource allocation matrix \mathbf{O} as input knowledge. A question naturally arises as to whether one can find a better observing schedule for the same telescopes with the same amounts of telescope time but with a different \mathbf{O} , i.e. whether one can add pulsars to or remove pulsars from schedules of certain telescopes to increase the detection significance? The configuration with all ${}^iO_\nu = 1$ allows one to use any telescope to observe any pulsar, i.e. allows one to adjust the schedule with the maximal degrees of freedom. In this way, the optimization schedule of configuration (${}^iO_\nu = 1$) leads to the highest GW detection significance. If any schedule has the same detection significance as the optimal schedule with all ${}^iO_\nu = 1$, we call such schedule ‘global optimal’. To determine whether the global optimization is achievable, we first investigate the case when the pulse jitter noise can be ignored, we then discuss situations where the pulse jitter noise becomes important.

When the pulse jitter noise is neglected, there is a close relation between the single telescope optimization and the multiple telescope optimization. In fact, under certain conditions, the optimization for multiple telescopes is equivalent to the single telescope optimization. To see this, we replace the variables ${}^iP_\nu$ and ${}^iO_\nu$ in equation (22) by *effective telescope time* ${}^i\tau_e$ as follows

$${}^i\tau_e = \sum_{\nu=1}^{N_{\text{tel}}} \mathcal{G}_\nu^2 {}^iP_\nu {}^iO_\nu. \quad (28)$$

After ignoring the σ_J , equation (22) becomes

$${}^i\sigma_w = {}^i\sigma_0 {}^i\tau_e^{-1/2}, \quad (29)$$

and the constrains equation (24) reduces to a single constraint

$$\sum_{i=1}^N {}^i\tau_e = \tau_e \equiv \sum_{\nu=1}^{N_{\text{tel}}} \tau_\nu \mathcal{G}_\nu^2. \quad (30)$$

By comparing equations (29) and (30) with equation (23) and (21), one can see that the optimization for multiple telescopes is very similar to the single telescope optimization. In fact, if there exists a unique solution of ${}^iP_\nu$ to equation (28), which satisfies each individual constraint of equation (24), the multiple telescope and single telescope optimization are mathematically identical.

The differences between multiple telescope and single telescope optimization lie in the difference between the constraints equation (24) and (30). For the single telescope case, only one constraint (equation 23) is involved. This is very different from the case of multiple telescopes, where N_{tel} constraints (equation 24) are present. The variable substitution in equation (28) combines all N_{tel} constraints (equation 24) and forms a single constraint (equation 30), where the constraint of each individual telescope is ignored. Whether global optimization is achievable is, now, equivalent to whether one can find a solution to ${}^iP_\nu$ for equation (28), while satisfying all individual constraints (equation 24).

Generally, when solving ${}^iP_\nu$ from equation (28) and

(24), one meets three types of situations: a unique solution, multiple solutions and no solution. For the case of multiple solutions, there are multiple choices for the optimal schedule. All these configurations are identical in the sense that they give the same GW detection significance. The case of no solution can only arise when constraints for some telescopes cannot be met, i.e. some of the pulsars need more time than the telescopes can give, while some of the pulsars have more telescope time than should be assigned. Take the case with two telescopes and two pulsars as an example, where the gain of the two telescopes are the same, two pulsars have identical σ_0 , and ${}^i\mathcal{O}_\nu = \begin{bmatrix} 1 & 1 \\ 0 & 1 \end{bmatrix}$, i.e. only the second telescope can observe the second pulsar. Since the two pulsars have the same σ_0 , the total effective telescope time should then also be the same for the optimal schedule (i.e. ${}^1\tau_e = {}^2\tau_e$). However if the first telescope does not have enough time, one gets ${}^1\tau_e < {}^2\tau_e$ and the global optimal schedule is not achievable for such configurations.

The case for which there no solution to equation (28), is due to an improper choice of telescopes. Most of the time the matrix \mathbf{O} is determined by the sky coverage of the telescopes. Thus, if no solution can be found, one needs to seek telescopes with the appropriate sky coverage or extend the time for telescopes with the sky coverage. In order to identify such a no-solution situation we show in Appendix D that a solution to equation (28) exists, if the following conditions are satisfied

$${}^i\tau_e \leq \sum_{\nu=1}^{N_{\text{tel}}} \mathcal{G}^2 \tau_\nu {}^i\mathcal{O}_\nu, \text{ for any index of pulsar } i. \quad (31)$$

One can identify which pulsar in equation (31) fails. These failures indicate the corresponding elements of resources allocation matrix to be adjusted.

We now consider the situation where the pulse jitter noise becomes important. Clearly, if we cannot ignore the pulse jitter noise, the effective telescope time is no longer linearly dependent on the telescope time ${}^iP_\nu$ as in equation (28) and we do not have a simple method to check if the global optimization is achieved. However we can still set all the ${}^i\mathcal{O}_\nu = 1$, find the global optimal strategy, and compare it with the optimal strategy for the input ${}^i\mathcal{O}_\nu$ to check if the global optimization is achieved.

In Figure 1, we give four examples for the optimization of multiple telescopes. In these examples, two telescopes are used to observe two pulsars, where the pulsar noise parameters and the telescope parameters are specified in Table 1. These four examples are given as follows. i) ‘Case A’, two identical pulsars are observed with two identical telescopes. The global optimal schedule is achievable and one can exchange telescope time between the two telescopes. As indicated in Figure 1, as long as we assign the same amount of effective telescope time ${}^i\tau_e$ for two pulsars, it is the optimal observing schedule. ii) ‘Case B’, telescope 1 has twice the gain compared to telescope 2. Similar to ‘case A’, the global optimal schedule is achievable and one can exchange telescope time. But due to the gain differences, the telescope time exchange should be weighted by the gain, such that the same amount of effective telescope time is assigned to the two identical pulsars. iii) ‘Case C’, where telescope 1 has more time (1.5 hr) available compared to telescope 2 (1 hr)

and only telescope 2 can be used to observe the 2nd pulsar (as indicated by the matrix ${}^i\mathcal{O}_\nu$). For this case, the total telescope time is the same as in ‘case A’, but we do not achieve the same low level of \mathcal{L} as in ‘case A’, i.e. global optimization is not achievable. This is due to the constraint from matrix ${}^i\mathcal{O}_\nu$, which prevents us from reaching the global optimization as discussed. iv) ‘Case D’, where pulsar 1 is affected by pulse jitter noise. In this case, one does not have the freedom to exchange telescope time and optimization suggests that the low gain telescope (telescope 2) should spend more time on the pulse jitter affected pulsar (pulsar 1).

4 RESULTS

As examples, we use pulsar properties measured from data of the PPTA, EPTA and NANOGrav to show the potential benefit of optimizing the observing schedule. The parameters of the pulsars are given in Table 2.

Figure 2 shows the comparison between the GW detection significance $\langle S \rangle$ for an unoptimized and an optimized PTA with the same parameters. We can see that the optimal observing strategy increases the GW detection significance. Evaluating from the rising edge of the curve, the optimized arrays are able to detect a GW background 2-3 times weaker than unoptimized arrays depending on the pulsar population. Because the radiometer noise $\sigma_0 \mathcal{G}^{-1}$ dominates over the pulse jitter noise for most pulsars using current timing techniques, we ignore the pulse jitter noise in these examples.

We also note that the larger the red noise level is, the less we gain from optimizing the observing schedule. When the amplitude of intrinsic red noises is large, the ${}^{ij}A$ dominates the detection significance as shown in equation (15), and thus the detection is no longer sensitive to the schedule optimization, which only affects the ${}^{ij}B$ terms. In fact, only if the pulsar noise level is sensitive to the observing schedule (i.e. when red noise does not dominate), the optimization will be effective. This conclusion applies to any type of GW detector.

In the optimization process, one always uses a numerical technique to determine the optimal observation plan. It is, nevertheless, worth finding a rule of thumb to determine an ‘approximate’ optimal strategy. We prove in Appendix C that, for strong GW cases, the optimal observing schedule weakly depends on the amplitude of the GW background and a good approximation for the optimal schedule is

$${}^i\tau = \tau \left(\frac{\sqrt{{}^iQ}}{\sum_{j=1, \neq i}^N \sqrt{{}^jQ}} \right), \quad (32)$$

where the iQ is defined as

$${}^iQ = {}^i\sigma_0^2 \mathcal{G}^{-2} + \sigma_J^2. \quad (33)$$

Here the iQ , noise parameter, defines the noisiness of the i -th pulsar observed using a telescope of gain \mathcal{G} .

By comparing the numerical optimization and the result from equation (32) in Figure 3, we show that the optimal schedule is insensitive to the GW amplitude and can be well approximated by equation (32), when the amplitude of the GW is large. For the case of a weak GW background, the optimal schedule for most of the pulsars is still close to equation (32), but the optimal schedule for noisy pulsars

Table 1. The telescope configurations and pulsar noise parameters for each case given in Figure 1. σ_0 and σ_J take the unit of second, τ takes the unit of hour, and the gain \mathcal{G} take an arbitrary fiducial unit as explained in the main text.

	case A:		case B:	
Radiometer noise	${}^1\sigma_0 = 10^{-7}$	${}^2\sigma_0 = 10^{-7}$	${}^1\sigma_0 = 10^{-7}$	${}^2\sigma_0 = 10^{-7}$
Jitter noise	${}^1\sigma_J = 0$	${}^2\sigma_J = 0$	${}^1\sigma_J = 0$	${}^2\sigma_J = 0$
Observation time	$\tau_1 = 1$	$\tau_2 = 1$	$\tau_1 = 1$	$\tau_2 = 1$
Telescope gain	$\mathcal{G}_1 = 1$	$\mathcal{G}_2 = 1$	$\mathcal{G}_1 = 2$	$\mathcal{G}_2 = 1$
Resource allocation matrix	${}^iO_\nu = \begin{bmatrix} 1 & 1 \\ 1 & 1 \end{bmatrix}$		${}^iO_\nu = \begin{bmatrix} 1 & 1 \\ 1 & 1 \end{bmatrix}$	
	case C:		case D:	
Radiometer noise	${}^1\sigma_0 = 10^{-7}$	${}^2\sigma_0 = 10^{-7}$	${}^1\sigma_0 = 10^{-7}$	${}^2\sigma_0 = 10^{-7}$
Jitter noise	${}^1\sigma_J = 0$	${}^2\sigma_J = 0$	${}^1\sigma_J = 10^{-7}$	${}^2\sigma_J = 0$
Observation time	$\tau_1 = 1.5$	$\tau_2 = 0.5$	$\tau_1 = 1$	$\tau_2 = 1$
Telescope gain	$\mathcal{G}_1 = 1$	$\mathcal{G}_2 = 1$	$\mathcal{G}_1 = 2$	$\mathcal{G}_2 = 1$
Resource allocation matrix	${}^iO_\nu = \begin{bmatrix} 1 & 1 \\ 0 & 1 \end{bmatrix}$		${}^iO_\nu = \begin{bmatrix} 1 & 1 \\ 1 & 1 \end{bmatrix}$	

Table 2. Parameters for PPTA, EPTA and NANOGrav pulsars taken from Hobbs et al. (2010). We assume that all the white noise is due to the radiometer noise and pulse jitter noise can be ignored.

PSR J	P (ms)	P_b (d)	S1400 (mJy)	Array	PPTA σ_0 (μ s)	EPTA σ_0 (μ s)	NANOGrav σ_0 (μ s)
J0030+0451	4.87	-	0.6	EPTA, NANOGrav	-	0.54	0.31
J0218+4232	2.32	2.03	0.9	NANOGrav	-	-	4.81
J0437-4715	5.76	5.74	142.0	PPTA	0.03	-	-
J0613-0200	3.06	1.20	1.4	PPTA, EPTA, NANOGrav	0.71	0.45	0.50
J0621+1002	28.85	8.32	1.9	EPTA	-	9.58	-
J0711-6830	5.49	-	1.6	PPTA	1.32	-	-
J0751+1807	3.48	0.3	3.2	EPTA	-	0.78	-
J0900-3144	11.1	18.7	3.8	EPTA	-	1.55	-
J1012+5307	5.26	0.60	3.0	EPTA, NANOGrav	-	0.32	0.61
J1022+1001	16.45	7.81	3.0	PPTA, EPTA	0.37	0.48	-
J1024-0719	5.16	-	0.7	PPTA, EPTA	0.43	0.25	-
J1045-4509	7.47	4.08	3.0	PPTA	2.68	-	-
J1455-3330	7.99	76.17	1.2	EPTA, NANOGrav	-	3.83	1.60
J1600-3053	3.60	14.35	3.2	EPTA, PPTA	0.32	0.23	-
J1603-7202	14.84	6.31	3.0	PPTA	0.70	-	-
J1640+2224	3.16	175.46	2.0	EPTA, NANOGrav	-	0.45	0.19
J1643-1224	4.62	147.02	4.8	PPTA, EPTA, NANOGrav	0.57	0.56	0.53
J1713+0747	4.57	67.83	8.0	PPTA, EPTA, NANOGrav	0.15	0.07	0.04
J1730-2304	8.12	-	4.0	PPTA, EPTA	0.83	1.01	-
J1732-5049	5.31	5.26	-	PPTA	1.74	-	-
J1738+0333	5.85	0.35	-	NANOGrav	-	-	0.24
J1741+1351	3.75	16.34	-	NANOGrav	-	-	0.19
J1744-1134	4.08	-	3.0	PPTA, EPTA, NANOGrav	0.21	0.14	0.14
J1751-2857	3.91	110.7	0.06	EPTA	-	0.90	-
J1824-2452	3.05	-	0.2	PPTA, EPTA	0.39	0.24	-
J1853+1303	4.09	115.65	0.4	NANOGrav	-	-	0.17
J1857+0943	5.37	12.33	5.0	PPTA, EPTA, NANOGrav	0.82	0.44	0.25
J1909-3744	2.95	1.53	3.0	PPTA, EPTA, NANOGrav	0.19	0.04	0.15
J1910+1256	4.98	58.47	0.5	EPTA, NANOGrav	-	0.99	0.17
J1918-0642	7.65	10.91	-	EPTA, NANOGrav	-	0.87	1.08
J1939+2134	1.56	-	10.0	PPTA, EPTA, NANOGrav	0.11	0.02	0.03
J1955+2908	6.13	117.35	1.1	NANOGrav	-	-	0.18
J2019+2425	3.94	76.51	-	NANOGrav	-	-	0.66
J2124-3358	4.93	-	1.6	PPTA	1.52	-	-
J2129-5721	3.73	6.63	1.4	PPTA	0.87	-	-
J2145-0750	16.05	6.84	8.0	PPTA, EPTA, NANOGrav	0.86	0.40	1.37
J2317+1439	3.44	2.46	4.0	NANOGrav	-	0.81	0.25

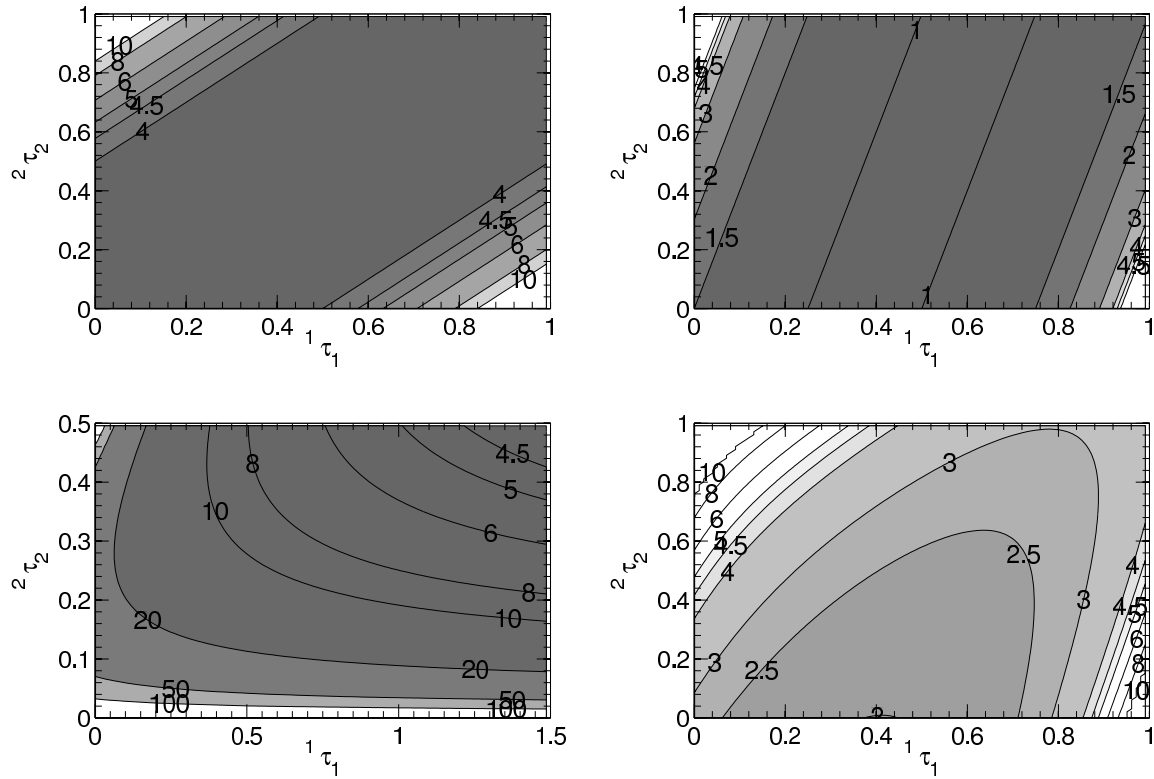


Figure 1. Four examples to illustrate the optimization of multiple telescopes. Here, we plot \mathcal{L} , defined in equation (25), as a function of telescope time. The smaller \mathcal{L} is, the better the observing schedule. In all examples, two pulsars are observed with two telescopes. The telescope configurations and pulsar noise parameters for each case is given in Table 1. The x-axis and y-axis are for the ${}^1\tau_1$, i.e. the time for the 1st telescope observing the 1st pulsar, and ${}^2\tau_2$, i.e. the time for the 2nd telescope observing the 2nd pulsar, respectively.

(pulsars with larger iQ) starts to deviate from the analytic approximation.

There are a few more general conclusions on improving the timing accuracy independent of GW detection algorithms. In order to improve timing accuracy, one can use telescopes with higher effective gain⁴ or increase telescope time. Increasing the telescope gain reduces σ_w and increasing telescope time reduces both σ_w and σ_J . The example of case ‘D’ in Figure 1 shows that one should use a low gain telescope on those pulsars with larger jitter noise level, while using a high gain telescope on pulsars with larger radiometer noise. This is further supported by the results in Figure 4, which shows that increasing the telescope time is more effective than using a high gain telescope for pulse jitter noise dominant pulsars.

Besides providing the optimal schedule to detect a GW background, our technique answers the question about the optimal *number* of pulsars one should observe in a PTA with a given amount of telescope time. The number of pulsars in a PTA has two effects on the GW detection significance. Firstly, from equation (15), one can see that the significance increases as $\langle S \rangle \propto \sqrt{M} \sim N$. Secondly, since the

telescope time is limited, observing more pulsars increases the TOA noise level, i.e. $\sigma_w^2 \propto N^{-1}$ given a fixed amount of telescope time. When N becomes large, the two effects mentioned above cancel each other out, and the detection significance becomes insensitive to N . In general, when the number of pulsars (N) is small, the detection significance increases with N . If all pulsars have the same noise level, the detection significance saturates for large N , where the saturation level is mainly determined by the available telescope time. In practice, when trying to include more pulsars in a timing array, pulsars with a higher noise level will be inevitably included, such that the detection significance will decrease for any GW detection algorithm. In this way, observing more pulsars does not necessarily help detecting the GW background, unless one gets more telescope time. Given the telescope time, the number of pulsars, at which the GW detection significance achieves its maximum, is the optimal number of pulsars one should use in the PTA. We propose the following algorithm to determine the best sample of pulsars to observe.

- (i) From a group of to-be-observed pulsars, choose the two pulsars with smallest noise levels, then optimize the schedule, and compute the GW detection significance.
- (ii) Include one extra pulsar, optimize the schedule, compute the GW detection significance, loop over the rest of

⁴ Here, telescopes with higher effective gain \mathcal{G} can be telescopes with larger collection area, lower system temperature, wider bandwidth and so on.

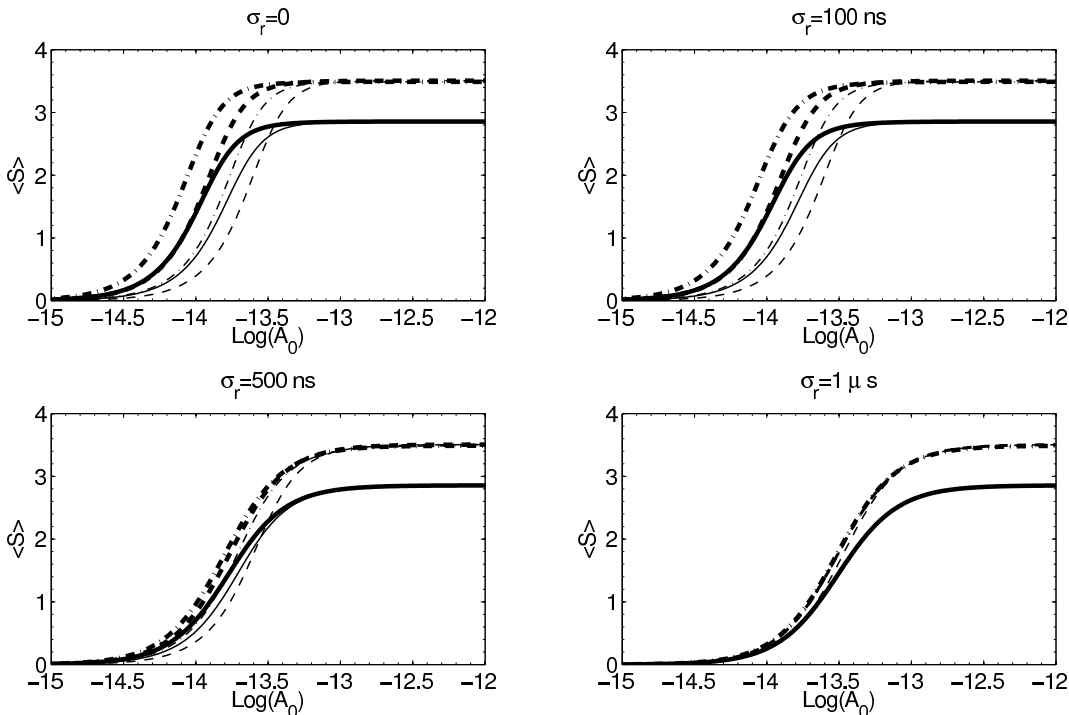


Figure 2. The GW background detection significance for PPTA, EPTA and NANOGrav with 5 year bi-weekly (one session every two weeks) observations. The white noise levels σ_0 are taken from Table 2 and the red noise levels σ_r are given above each panel. The x-axis shows the characteristic strain A_0 of the GW background with spectral index of $\alpha = -2/3$. The y-axis shows the expected detection significance $\langle S \rangle$. The solid lines, dashed lines, and dashed-dotted lines are for PPTA, EPTA and NANOGrav respectively. The thick lines are the optimized cases, while the thin lines are the unoptimized versions. Here, the constraint is the observation time, i.e. for each project, the total amount of observing time of each session is fixed to be 20 hours. If the red noise level is zero, the optimized array is able to detect 2-3 times weaker GW signals compared to its unoptimized version depending on the pulsar population.

the pulsars and find the new pulsar leading to the largest detection significance.

(iii) If the GW detection significance increases by including the new pulsar, add this pulsar to the list, and repeat the second step for the rest of the pulsars, otherwise the optimal set of pulsars is already achieved.

When pulsar surveys discover a new pulsar, we can check whether it is worth including it in the PTA by using the above algorithm, although, to start with, sufficient observations are still necessary to measure the noise properties of this pulsar.

5 DISCUSSIONS AND CONCLUSIONS

In this paper, we have investigated a technique to optimize the allocation of telescope time in a pulsar timing array to maximize the GW detection significance given a fixed amount of telescope time. This is done in two steps. First, the GW detection significance using a correlation detector is calculated analytically as a function of the white noise and red noise level of each pulsar, i.e. equation (15). Secondly, the GW detection significance is optimized under the constraints that the allocated telescope time is fixed. The constrained optimization is converted to a corresponding constraint-free optimization using the coordinate transfor-

mations of equation (26) and (27). Finally, the optimization is solved numerically using the downhill simplex algorithm. For characteristic PTAs, the optimized arrays are able to detect a GW background 2-3 times weaker than unoptimized arrays depending on the pulsar population. Besides the single telescope case, we also derive the optimization algorithm for multiple telescopes. We also examine the links between the multiple and single telescope optimization. We investigate the optimal number of pulsars to observe for a given PTA, where the algorithm to construct the optimal group of pulsars from candidates is also included.

In our optimization, the total telescope time τ and τ_ν are input parameters, that need to be determined before optimizing the schedule. When defining a PTA project, one can start with a reasonable amount of telescope time, say 20 hours per each session/telescope, optimize the schedule, calculate the detection significance $\langle S \rangle$, check if the detection is sensitive enough to the predicted GW background, and then adjust the input total telescope time accordingly, i.e. increase total telescope time, if the PTA is not sensitive enough.

In practice, the detailed numerical values for the optimal observing strategy are still to-be-determined, due to the lack of measurements for the necessary pulsar noise parameters. To determine the realistic optimization strategy, these parameters are critical. A detailed investigation on the indi-

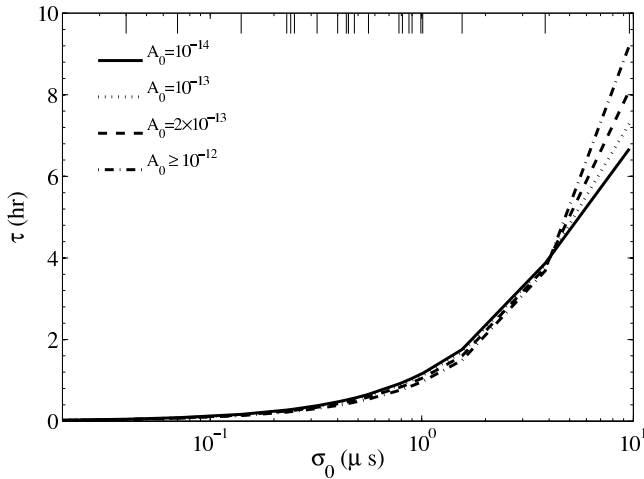


Figure 3. The optimal telescope time for each pulsar as a function of its white noise level. The x-axis shows the one-hour pulsar noise level σ_0 . The y-axis shows the optimal telescope time for the pulsar per observing session. The EPTA pulsars are used in this demonstration, where the total telescope time is 24 hours, i.e. the average telescope time for each pulsar is 1 hour. We indicate σ_0 for each pulsar using a vertical line on the top of the figure. The dotted-dashed line, dashed line, dotted line and solid line are for optimization results with GW amplitude of $A_0 = 10^{-12}, 10^{-13}, 2 \times 10^{-13}$, and 10^{-14} respectively. The results of equation (32) overlaps with the dotted-dashed line. For GWs with amplitude between 10^{-12} and 10^{-13} , the optimal schedules are very close to each other. For the weaker GW cases, e.g. $A_0 = 10^{-14}$, the optimal schedule starts to deviate from the approximation equation (32). Such a deviation is mainly due to the pulsars with a high noise level. Since these noisy pulsars will not contribute significantly to the GW signal detection, the optimal algorithm starts to reduce its observing time. For most of the pulsars, the optimal schedule is still close to the result from equation (32).

vidual timing properties of potential PTA pulsars is highly necessary, from which further observations will benefit.

One may encounter the situation, in which the optimal strategy requires longer observing time for certain pulsars per session than their transit time. If this happens, one has to split one observing session into several successive sessions. The GW detection significance is not significantly impaired by session splitting, since the GW induced timing signal has a very red spectrum and we are detecting its low frequency component. However the session splitting can lead to inconveniences in practical arrangements. A better way to avoid such a situation is to construct the PTA using telescopes with enough geographical coverage, which can be one of the driving reasons for the IPTA project.

The optimization in this paper is designed to maximize the GW detection significance. Our optimization is built for the correlation detector proposed by Jenet et al. (2005). As shown in Appendix C, our optimization, which is very close to minimizing the total PTA noise power, can be different from optimization for other types of GW detectors e.g. frequentist detectors (Verbiest et al. 2009; Yardley et al. 2011) or the Bayesian detector (van Haasteren et al. 2009, 2011). In fact, as already shown by Burt et al. (2011), one can get a different optimal observation schedule, when focusing on single source detection. We have ignored the information of

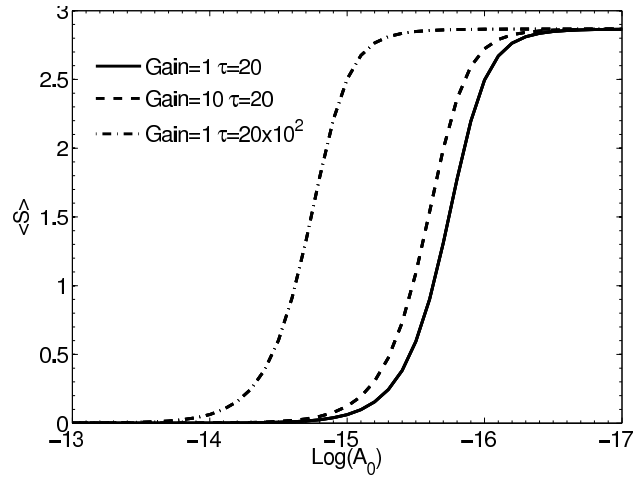


Figure 4. The GW detection significance $\langle S \rangle$ (y-axis) as a function of GW amplitude $\log(A_0)$ (x-axis), given different telescope gain and amount of telescope time. In the calculation, we assume that the PTA is composed of 20 pulsars, all of which have $\sigma_0 = 100$ ns and $\sigma_J = 100$ ns. We plot three telescope configurations here, each of which is labeled with the numerical value of total telescope time τ and telescope gain \mathcal{G} . Here the telescope time is in units of hours, the gain takes an arbitrary fiducial unit as in equation (21). For the following two PTA configurations, the $\{\mathcal{G} = 10, \tau = 20\}$ and the $\{\mathcal{G} = 1, \tau = 20 \times 10^2\}$, all pulsars have the same level of radiometer noise, which is 10 times smaller than the case where $\{\mathcal{G} = 1, \tau = 1\}$. However, because of the pulse jitter noise effect, the configurations with more telescope time performs better than the cases with higher system gain. Furthermore, by comparing $\{\mathcal{G} = 10, \tau = 20\}$ case with the case of $\{\mathcal{G} = 1, \tau = 20 \times 10^2\}$, we conclude that it is important, even for a high gain telescope, to acquire sufficient telescope time in order to improve the GW detection significance, when the pulsar becomes pulse jitter noise dominant.

historical non-overlapping data in our algorithms, because the non-overlapping data has very limited contributions to the cross-power of GW signals, although these data can be important to constrain the upper limit of GW amplitude (van Haasteren et al. 2011). Furthermore, the PTA offers an opportunity to investigate much broader topics, e.g. interstellar medium effects, time metrology, and so on. This paper, thus, by no means claims that our objective function is the only one we should pursue. However our basic framework of optimization, constraints and related numerical techniques will be the same for other detectors. It is straightforward to generalize our method to these detectors. For Bayesian detectors, there is no analytical expression for the detection significance at present. The Bayesian detectors are usually computationally expensive, which makes the optimization difficult at this stage.

Figure 2 shows that increasing the levels of red noise does not decrease the saturation level of the detection significance, i.e. the detection significance at large GW amplitude. This seems to contradict the conclusion of Jenet et al. (2005) and Verbiest et al. (2009), where the red spectrum of the GW limits the saturation level. As shown in equation (15), the term limiting the saturation level is due to the term $(1 + H(\theta))\gamma_{kk'}^2$ in ${}^{ij}A$, which is the non-zero correlation between GW signals of two different pulsars. Since

the red intrinsic noise of pulsars, unlike the GW induced signal, are uncorrelated, it is natural that they do not limit the saturation level.

In this paper, we use a phenomenological model to describe the noise component, which is a superposition of a telescope-time dependent white noise component and another red noise component independent of telescope time. The reason for using such a phenomenological model is to use the observational information and to introduce minimal theoretical assumptions. Our white noise term contains both the radiometer noise and pulse jitter noise. Although the radiometer noise is the current bottleneck in timing accuracy of most MSPs ($\sigma_0 \mathcal{G}^{-1} \gg \sigma_J$), the pulse jitter noise (Liu et al. 2011), can be a potential limitation for future single dish high gain telescopes. Similarly, red noise can be another limitation for the long term timing accuracy. Detailed studies on the pulse jitter noise and red noise properties and related mitigation algorithms will be useful for the future prospects of GW detection.

We assumed that the noise sources are not correlated among pulsars. This may be valid for all the noise of astrophysical origin, although the clock error can be an identical noise among all pulsars (Hogan & Rees 1984; Foster & Backer 1990; Manchester 1994; Tinto 2011). The clock error may also introduces correlations in TOAs from different telescopes, since observatory clocks are usually synchronized. However, thanks to the red spectrum of most clock errors (Riehle 2004), one can completely remove the noise using simultaneous differential measurements (Tinto 2011). Furthermore, as we argue in Appendix E, such a common noise source can be significantly suppressed by post processing, if each session is compact within the time scale of days. In this way, our assumption is justified that different noise sources are not correlated among pulsars.

Our optimal observation strategy is for allocating telescope time among pulsars. This only affects the white noise related part (${}^{ij}B$ terms) in GW detection significance (equation (15)). In fact, one can also specify the epoch of each session to minimize the effect of the red noise related part (${}^{ij}A$ terms). Since these ${}^{ij}A$ terms can be more effectively reduced using whitening techniques (Jenet et al. 2005, 2006), we do not optimize the epoch of each session to avoid sampling artifacts and to reduce the complexities in observation management. The discussions for the frequency of observation sessions are omitted, since it is not bounded in terms of optimization, i.e. observing more frequently sessions simply increase the sensitivity.

ACKNOWLEDGMENTS

We gratefully acknowledge support from the ERC Advanced Grant ‘LEAP’, Grant Agreement Number 227947 (PI Michael Kramer). We thank Norbert Wex for reading through the manuscript and his useful discussions. We also thank the anonymous referee for the important and helpful comments.

REFERENCES

Burt B. J., Lommen A. N., Finn L. S., 2011, ApJ, 730, 17

Cordes J. M., Shannon R. M., 2010, arxiv: 10103785
 Ferdman R. D., van Haasteren R., Bassa C. G., et al. 2010, Classical and Quantum Gravity, 27, 084014
 Foster R. S., Backer D. C., 1990, ApJ, 361, 300
 Hellings R. W., Downs G. S., 1983, ApJL, 265, L39
 Hobbs G., et al. 2010, Classical and Quantum Gravity, 27, 084013
 Hobbs G. B., et al., 2009, PASA, 26, 103
 Hogan C. J., Rees M. J., 1984, Nature, 311, 109
 Jaffe A. H., Backer D. C., 2003, ApJ, 583, 616
 Janssen G. H., et al., 2008, A&A, 490, 753
 Jenet F., Finn L. S., Lazio J., et al. 2009, ArXiv e-prints
 Jenet F. A., et al., 2006, ApJ, 653, 1571
 Jenet F. A., Hobbs G. B., Lee K. J., Manchester R. N., 2005, ApJL, 625, L123
 Kramer M., Stappers B., 2010, in ISKAF2010 Science Meeting - ISKAF2010, June 10-14, 2010 Assen, the Netherlands LOFAR, LEAP and beyond: Using next generation telescopes for pulsar astrophysics . p. 10
 Kramer M., Wielebinski R., Jessner A., Gil J. A., Seiradakis J. H., 1994, A&A, 107, 515
 Lazaridis K., 2010, preprint (astro-ph/1002.0737)
 Lee K., Jenet F. A., Price R. H., Wex N., Kramer M., 2010, ApJ, 722, 1589
 Lee K. J., Jenet F. A., Price R. H., 2008, ApJ, 685, 1304
 Liu K., Keane E. F., Lee K. J., Kramer M., Cordes J. M., Purver M. B., 2012, MNRAS, 420, 361
 Liu K., Verbiest J. P. W., Karmmer M., Stappers B. W., van Straten W., Cordes J. M., 2011, submitted
 Manchester R. N., 1994, Proceedings of the Astronomical Society of Australia, 11, 1
 Manchester R. N., 2008, in C. Bassa, Z. Wang, A. Cumming, & V. M. Kaspi ed., 40 Years of Pulsars: Millisecond Pulsars, Magnetars and More Vol. 983 of American Institute of Physics Conference Series, The Parkes Pulsar Timing Array Project. pp 584–592
 Nan R., Wang Q., Zhu L., Zhu W., Jin C., Gan H., 2006, Chinese Journal of Astronomy and Astrophysics Supplement, 6, 020000
 Nelder J. A., Mead R., 1965, The Computer Journal, 7, 303
 Riehle F., 2004, Frequency Standards: Basics and Applications. Wiley-VCH
 Rodin A. E., 2011, Astronomy Reports, 55, 132
 Sesana A., Haardt F., Madau P., Volonteri M., 2004, ApJ, 611, 623
 Shannon R. M., Cordes J. M., 2010, ApJ, 725, 1607
 Smits R., Kramer M., Stappers B., Lorimer D. R., Cordes J., Faulkner A., 2009, A&A, 493, 1161
 Smits R., Lorimer D. R., Kramer M., Manchester R., Stappers B., Jin C. J., Nan R. D., Li D., 2009, A&A, 505, 919
 Stappers B. W., Kramer M., Lyne A. G., D’Amico N., Jessner A., 2006, Chinese Journal of Astronomy and Astrophysics Supplement, 6, 020000
 Tinto M., 2011, Phy. Rev. Lett., 106, 191101
 van Haasteren R., Levin Y., 2012, preprint (astro-ph/1202.5932)
 van Haasteren R., Levin Y., Janssen G. H., et al., 2011, MNRAS, 414, 3117
 van Haasteren R., Levin Y., McDonald P., Lu T., 2009, MNRAS, 395, 1005
 Verbiest J. P. W., et al., 2009, MNRAS, 400, 951

Verbiest J. P. W., et al., 2010, *Classical and Quantum Gravity*, 27, 084015

Yardley D. R. B., et al., 2011, *MNRAS*, 414, 1777

Zee A., 2010, *Quantum Field Theory in a Nutshell: Second Edition*. Princeton University Press, 2nd ed

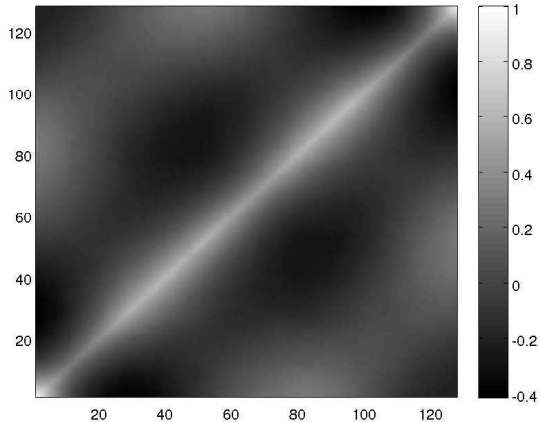


Figure A1. The correlation coefficient for 128 regular samples of a red noise power-law. For illustration purposes the spectral index is -2 and we removed the fitted parabolic term in the signal $s(t_i)$. The x-axis and y-axis show the index i and j , respectively. The colors indicate values of the correlation coefficients. The diagonal elements of the plot are not equal to each other. This clearly show that the polynomial fitting breaks the stationarity of the red noise.

APPENDIX A: PULSAR TIMING CORRELATION

In this section, we calculate the cross correlation for a Gaussian random signal with a power-law spectrum. We discuss two main issues arising in the calculation, the effect of polynomial fitting on the cross correlation and the effects of spectral leakage. For a stationary continuous-in-time random signal $s(t)$, which has a prescribed power spectrum of $S_s(f)$, the well-known Wiener-Khinchin theorem states that the autocorrelation $\langle s(t_i)s(t_j) \rangle$ is the Fourier transform of the power spectral density, i.e.

$$\langle s(t_i)s(t_j) \rangle = \int_0^\infty S_s(f) e^{2\pi f(t_i - t_j)} df. \quad (\text{A1})$$

However due to the fitting of polynomials, the direct application of the above to the pulsar timing problem needs revision.

In a practical pulsar timing data reduction pipeline, one usually uses a least-square polynomial fitting to extract the pulsar parameters. Such a fit is *not* a stationary process, which prevents us from calculating the correlation directly using equation (A1). In this paper, correlations are calculated via numerical simulations, that take the following steps: i) Generate a series of the sampled signal using individual frequency components as described in Lee et al. (2008) ii) Fit the signal with a polynomial to simulate the effects of fitting the pulsar rotation frequency and its derivative. iii) Calculate the required cross correlation. iv) Repeat steps (i), (ii), (iii) and average the cross correlation, until the required precision is attained. In this paper, the correlations are calculated to a relative error of 1%. From the numerical results in Figure A1, the polynomial fitting clearly breaks the stationarity of signals.

The other issue is the spectral leakage. A red noise signal with a steep spectrum introduces leakage from low frequency components into high frequency components. For a

red noise signal with a spectral density of $S_s(f) \sim f^{-\beta}$, the amplitude for those signal components within the frequency range $[f, f + \delta f]$ is $f^{-\beta/2} \delta f^{1/2}$. The waveform of this component will be sinusoidal, i.e. $s(t) \simeq f^{-\beta/2} \delta f^{1/2} \exp(2\pi f i t)$. At the low frequency limit, where $ft \ll 1$, $s(t)$ can be approximated using Taylor series

$$s(t) \sim f^{-\beta/2} \delta f^{1/2} \exp(2\pi i f t) \simeq \delta f^{1/2} \sum_{l=0}^{\infty} \frac{(2\pi i t)^l f^{l-\beta/2}}{l!}. \quad (\text{A2})$$

If we fit the waveform with a n degree polynomial, we effectively remove the leading terms up to $f^{n+3/2-\beta/2}$. Clearly, if $n + 3/2 - \beta/2 \leq 0$, the signal amplitude goes to infinity, when $f \rightarrow 0$. Thus there will be no low frequency cut-off in the spectrum, even for data with a finite length. In this case, the low frequency components are always dominant. To guarantee that the low frequency cut-off rises naturally (regularize the signal), we need to fit the time series to a polynomial with degree $n > \beta/2 - 3/2$. For example, the SMBH GW background introduces a pulsar timing signal with a spectral index of $\beta = 13/3$, hence we need at least $n = 1$, i.e. fitting with a first order polynomial (a straight line), although the spectral leakage from low frequency components is dominant.

We now take a closer look at the effects of the fitting on the RMS level of a signal with a power-law spectrum given by

$$S_s(f) = S_0 f^{-\beta}, \text{ with } f \in [f_L, \infty), \quad (\text{A3})$$

where the f_L is the lowest frequency cut-off, S_0 is the power spectrum value at the unit frequency. Using the data length (T) as the temporal unit, the RMS level of such signal is

$$\sigma^2 = S_0 T^{\beta-1} \frac{f_{0,L}^{1-\beta}}{(\beta-1)}, \quad (\text{A4})$$

where $f_{0,L} = T f_L$ is the dimensionless lowest cut-off frequency.

The polynomial fitting to regular sampled data using a ℓ^2 -norm is equivalent to the following *linear time-variant* filter

$$h(t_1, t_2) = \sum_{l=0}^n (2l+1) P_l(2t_1-1) P_l(2t_2-1), \quad (\text{A5})$$

where $t_1, t_2 \in [0, 1]$ are dimensionless time, n is the order of the fitting polynomial, and $P_l(\cdot)$ is the l -th order Legendre polynomial. Denoting the signal as $s(t)$ and the polynomial fitting of such a signal as $s_0(t)$, we have

$$s_0(t) = \int_0^1 h(t, t_2) s(t_2) dt_2, \quad (\text{A6})$$

and the residual is $s'(t) = s(t) - s_0(t)$.

The average RMS level of post-fitting residual becomes

$$\sigma'^2 = \int_0^1 dt s'(t)^2 = \int_0^1 \int_0^1 \int_0^1 h(t, t_1) h(t, t_2) s(t_1) s(t_2) dt dt_1 dt_2. \quad (\text{A7})$$

One can show that

$$\sigma'^2 = \sigma^2 - \int_0^1 \int_0^1 \sum_{l=0}^n (2l+1) P_l(2t_1-1) P_l(2t_2-1) C(t_1-t_2) dt_1 dt_2, \quad (\text{A8})$$

where $C(t_1 - t_2) = \langle s(t_1)s(t_2) \rangle$. For the case of a power-law spectrum, we have

$$C(t) = S_0 T^{\beta-1} \frac{f_{0,L}^{1-\beta}}{\beta-1} {}_1F_2 \left(\frac{1-\beta}{2}; \frac{1}{2}, \frac{3-\beta}{2}; -\pi^2 f_{0,L}^2 t^2 \right) + T^{\beta-1} (2\pi)^{\beta-1} \Gamma(1-\beta) \sin \left(\frac{\pi\beta}{2} \right) |t|^{\beta-1}, \quad (\text{A9})$$

where τ is dimensionless time in units of T , ${}_1F_2(\cdot)$ is the generalized hypergeometric function (see also van Haasteren et al. (2011) for the series presentation), and $\Gamma(\cdot)$ is the gamma function.

Integrating equation (A8), one reads

$$\begin{aligned} \sigma'^2 &= S_0 T^{\beta-1} \left[\right. \\ &- \sum_{k=n+1}^{\infty} \frac{(2\pi)^{2k} (-1)^{k+n} f_{0,L}^{2k+1-\beta} (1+n) \Gamma(k) \sin(\pi\beta)}{(1+2k-\beta) \Gamma(2+2k) \Gamma(k-n) \Gamma(2+k+n)} \\ &\left. + 2^{\beta-2} (1+n) \pi^{\beta-1} \frac{\Gamma(\frac{3+2m-\beta}{2}) \Gamma(\frac{\beta-1}{2}) \Gamma(\frac{1+\beta}{2})}{\Gamma(\frac{3+2n+\beta}{2}) \Gamma(1+\beta)} \right] \quad (\text{A10}) \end{aligned}$$

Clearly, if $2n+3 \geq \beta$, we have

$$\lim_{f_{0,L} \rightarrow 0} \sigma'^2 = S_0 T^{\beta-1} 2^{\beta-2} (1+n) \pi^{\beta-1} \frac{\Gamma(\frac{3+2m-\beta}{2}) \Gamma(\frac{\beta-1}{2}) \Gamma(\frac{1+\beta}{2})}{\Gamma(\frac{3+2n+\beta}{2}) \Gamma(1+\beta)}, \quad (\text{A11})$$

i.e. the RMS σ'^2 is regularized to be a finite value for $f_{0,L} \rightarrow 0$, which confirms our previous estimation. Usually pulsar spin and spin-down are subtracted from the data. This corresponds to the case of $n=2$. For GW induced signal, we have $\beta=13/3$ and $S_0 = h_c^2 (\text{yr}^{-1}) (12\pi^2)^{-1} \text{yr}^{-4/3}$, which gives

$$\sigma'^2 = h_c^2 (\text{yr}^{-1}) \frac{3^6 (2\pi)^{4/3} T^{10/3} \Gamma(\frac{2}{3})}{2^7 \cdot 5 \cdot 7^2 \cdot 11 \cdot 13} \text{yr}^{-4/3} \quad (\text{A12})$$

$$\simeq 2.55 \times 10^{-3} h_c^2 T^{10/3} \text{yr}^{-4/3}. \quad (\text{A13})$$

This is identical to the results of van Haasteren & Levin (2012).

It should be also noted that for such case ($\beta=13/3$ and $S_0 = h_c^2 (\text{yr}^{-1}) (12\pi^2)^{-1} \text{yr}^{-4/3}$) equation (A4) becomes

$$\sigma^2 \simeq 2.53 \times 10^{-3} h_c^2 T^{10/3} f_{0,L}^{-10/3} \text{yr}^{-4/3}. \quad (\text{A14})$$

In this way, estimating RMS value of fitted signal using equation (A4) is accurate enough for practical purposes, given data length is adopted as the *effective cut-off frequency*, i.e. to use $f_{0,L} = 1$.

APPENDIX B: GW DETECTION SIGNIFICANCE

In this section, we calculate the GW detection significance. The expected value for the detection significance $\langle S \rangle$ depends on Σ_c and $\langle {}^{ij}c \rangle$ as shown in equation (12). We determine the $\langle {}^{ij}c \rangle$ first. From equation (7), we have

$$\langle {}^{ij}c \rangle = \frac{1}{m} \sum_{k=1}^m \langle {}^i R_k {}^j R_k \rangle = \sigma_g^2 H({}^{ij}\theta). \quad (\text{B1})$$

To determine Σ_c , we need $\langle {}^{ij}c^2 \rangle$, which is calculated in a similar fashion such that

$$\langle {}^{ij}c^2 \rangle = \frac{1}{m^2} \left\langle \sum_{k=1}^m \sum_{k'=1}^m {}^i R_k {}^j R_k {}^{i'} R_{k'} {}^{j'} R_{k'} \right\rangle, \quad (\text{B2})$$

After using the correlation relation equation (3), equation (6), and performing the Wick expansion (Zee 2010) to calculate higher momentum, we have

$$\left\langle \frac{1}{m^2} \sum_{k=1}^m \sum_{k'=1}^m {}^i R_k {}^j R_k {}^{i'} R_{k'} {}^{j'} R_{k'} \right\rangle = \sigma_g^4 \left({}^{ij}A + {}^{ij}B + H({}^{ij}\theta)^2 \right). \quad (\text{B3})$$

The Σ_c is then

$$\begin{aligned} \Sigma_c &= \sqrt{\left\langle \frac{1}{M} \sum_{i-j \text{ pairs}} \left({}^{ij}c - \overline{\langle c \rangle} \right)^2 \right\rangle} \\ &= \sqrt{\frac{1}{M} \sum_{i-j \text{ pairs}} \left(\langle {}^{ij}c^2 \rangle - \overline{\langle c \rangle}^2 \right)} \\ &= \sigma_g^2 \sqrt{\Sigma_H^2 + \frac{1}{M} \sum_{i-j \text{ pairs}} \left({}^{ij}A + {}^{ij}B \right)}, \quad (\text{B4}) \end{aligned}$$

with which one can derive equation (15).

APPENDIX C: OPTIMIZATION USING LAGRANGIAN MULTIPLIER

In section 3, we describe the optimization technique using variable transformation and numerical optimization. In this section, we introduce another method solving the constrained optimization problem directly. As an example, we present the technique for the single telescope situation, which is also readily generalized.

The optimization problem for the single telescope case is to search the minimal value of $\mathcal{L} = \sum_{i-j \text{ pairs}} {}^{ij}B$ under the constraint that $\tau = \sum_{i=1}^n {}^i\tau$. Using a Lagrangian multiplier λ , we can re-cast the optimization problem to optimize the \mathcal{L}' , where

$$\mathcal{L}' = \mathcal{L} + \lambda \left(\tau - \sum_{i=1}^n {}^i\tau \right) \quad (\text{C1})$$

$$= \sum_{i-j \text{ pairs}} \frac{{}^i\kappa {}^j q}{j\tau} + \frac{{}^j\kappa {}^i q}{i\tau} + \frac{{}^i q {}^j q}{i\tau j\tau} + \lambda \left(\tau - \sum_{i=1}^n {}^i\tau \right) \quad (\text{C2})$$

where ${}^i q = ({}^i\sigma_0^2 \mathcal{G}^{-2} + {}^i\sigma_J^2) \sigma_g^{-2}$ and ${}^i\kappa = 1 + {}^i\sigma_r^2 \sigma_g^{-2}$. The minimization of \mathcal{L}' can be found by

$$\frac{\partial \mathcal{L}'}{\partial {}^i\tau} = 0, \quad (\text{C3})$$

$$\frac{\partial \mathcal{L}'}{\partial \lambda} = 0, \quad (\text{C4})$$

which give

$$\frac{{}^i q}{i\tau^2} \sum_{j=1, \neq i}^n j\kappa + \frac{{}^j q}{j\tau^2} \sum_{i=1, \neq j}^n i\kappa - \frac{\lambda}{2} = 0, \quad (\text{C5})$$

and

$$\sum_{i=1}^n {}^i\tau - \tau = 0. \quad (\text{C6})$$

It is easy to check that equation (C5) and (C6) can be solved using the following recipe:

1. Guess an initial value for ${}^i\tau$.
2. Update ${}^i\tau$ with a newer value using

$$\tau \frac{\sqrt{{}^i q \sum_{j=1, \neq i}^n (j\kappa + jq/j\tau)}}{\sum_{i=1}^n \sqrt{{}^i q \sum_{j=1, \neq i}^n (j\kappa + jq/j\tau)}} \rightarrow {}^i \tau \quad (C7)$$

3. Repeat step 2, until the required precision is achieved.

One can monitor the change of ${}^i \tau$ for each iteration until it converges to the necessary precision. The initial value for the iteration is determined from the strong-signal limit, i.e. ${}^i q \rightarrow 0$, where the iteration equation (C7) reduces to a solution

$${}^i \tau = \tau \frac{\sqrt{{}^i q \sum_{j=1, \neq i}^n j\kappa}}{\sum_{i=1}^n \sqrt{{}^i q \sum_{j=1, \neq i}^n j\kappa}} + \mathcal{O}(q). \quad (C8)$$

It is worthwhile noting that, in fact, the iteration process (equation (C7)) will not change the results very much from the initial value equation (C8). This is due to

$$\begin{aligned} & \tau \frac{\sqrt{{}^i q \sum_{j=1, \neq i}^n (j\kappa + jq/j\tau)}}{\sum_{i=1}^n \sqrt{{}^i q \sum_{j=1, \neq i}^n (j\kappa + jq/j\tau)}} \\ & \simeq \tau \frac{\sqrt{{}^i q \sum_{j=1}^n (j\kappa + jq/j\tau)}}{\sum_{i=1}^n \sqrt{{}^i q \sum_{j=1}^n (j\kappa + jq/j\tau)}} + \mathcal{O}\left(\frac{1}{n}\right) \\ & = \tau \frac{\sqrt{{}^i q}}{\sum_{i=1}^n \sqrt{{}^i q}} \\ & = \tau \frac{\sqrt{{}^i Q}}{\sum_{i=1}^n \sqrt{{}^i Q}}, \end{aligned} \quad (C9)$$

where ${}^i Q = {}^i \sigma_0^2 \mathcal{G}^{-2} + \sigma_j^2$. Clearly, the initial value equation (C8) we use is already a good approximation to the optimal observation strategy.

APPENDIX D: THE CONDITION OF EXISTING SOLUTIONS TO ${}^i P_\nu$

In this section, we investigate the conditions to be satisfied such that the following equations have solution ${}^i P_\nu$ for given ${}^i \tau_e, \mathcal{G}_\nu, {}^i O_\nu$, and τ_ν ,

$$\begin{cases} {}^i \tau_e = \sum_{\nu=1}^{N_{\text{tel}}} \mathcal{G}_\nu^2 {}^i P_\nu {}^i O_\nu, & (D1) \end{cases}$$

$$\begin{cases} \tau_\nu = \sum_{i=1}^N {}^i P_\nu {}^i O_\nu, & (D2) \end{cases}$$

$$\begin{cases} {}^i P_\nu \geq 0, & (D3) \end{cases}$$

where i is $1 \dots N$, ν is $1 \dots N_{\text{tel}}$, and ${}^i \tau_e$ satisfies equation (28).

We want to prove that equation (D1), (D2), and (D3) have solutions ${}^i P_\nu$, if and only if, for any i , the following condition is satisfied,

$${}^i \tau_e \leq \sum_{\nu=1}^{N_{\text{tel}}} \mathcal{G}_\nu^2 \tau_\nu {}^i O_\nu. \quad (D4)$$

The proof contains two steps as follows: i) The ‘only if’

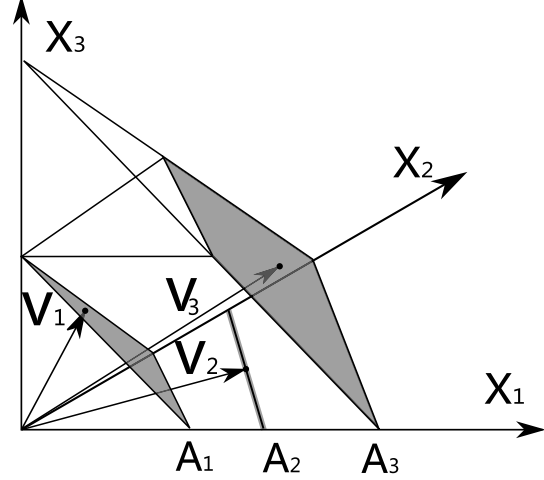


Figure D1. The illustration for the accessible region of the summation of vectors. Here X_1, X_2, X_3 are the coordinates. Because of the ${}^i O_\nu$ we choose, the vector v_1 is constrained to the region A_1 (the plane constrained to the shaded triangle) and the vector v_2 is constrained to the region A_2 (the line segment). The accessible region for the summation ($v_3 = v_1 + v_2$) of two vectors is clearly the A_3 , i.e. a plane with extra constraints.

part. If ${}^i P_\nu$ is the solution, then

$${}^i \tau_e = \sum_{\nu=1}^{N_{\text{tel}}} \mathcal{G}_\nu^2 {}^i P_\nu {}^i O_\nu \leq \sum_{\nu=1}^{N_{\text{tel}}} \mathcal{G}_\nu^2 \tau_\nu {}^i O_\nu, \quad (D5)$$

where the second step is due to the constraint of equation (D2) and (D3). ii) The ‘if’ part. It is easy to note that, under the constraints of equation (D2), any linear combination of the column vectors, e.g. $\beta_i = \sum_{\nu} c_\nu {}^i P_\nu {}^i O_\nu$, belongs to a hyperplane \mathcal{S} , because $\sum_{i=1}^N \beta_i = \sum_{\nu} \tau_\nu c_\nu$. Due to equation (D3), only part of the hyperplane \mathcal{S} is accessible to the vector β_i , i.e. β_i is constrained by $0 \leq \beta_i \leq \sum_{\nu} c_\nu \tau_\nu {}^i O_\nu$ in the \mathcal{S} . Denoting such an accessible region as \mathcal{A} , and let $c_\nu = \mathcal{G}_\nu^2$. Clearly, if the vector ${}^i \tau_e$ is in the accessible region \mathcal{A} , there exists a solution to equation (D1), which satisfies both equation (D2) and (D3). From equation (28), we know $0 \leq {}^i \tau_e \leq \sum_{\nu=1}^{N_{\text{tel}}} \mathcal{G}_\nu^2 \tau_\nu {}^i O_\nu$, thus the vector ${}^i \tau_e$ belongs to the accessible region \mathcal{A} , and the solution exists.

A graphical illustration for the condition is given in Fig-

ure D1, where we choose ${}^i O_\nu = \begin{bmatrix} 1 & 1 \\ 1 & 1 \\ 1 & 0 \end{bmatrix}$.

APPENDIX E: COMMON NOISE MITIGATION

Clock errors and other common noise sources are harmful to PTA observations. Tinto (2011) has shown that a simultaneous differential measurement of a pulsar TOA completely removes the clock error. Instead of the requirement for simultaneous observations of multiple pulsars, we argue in this section that one can still remove most of the clock errors in post processing without simultaneity, if each observation session is compact enough.

Suppose the pulsar timing signal contains an identical (clock) noise $n_c(t)$ with a red spectrum. A subtraction between the timing signals of two different pulsars at two

close epochs will remove most power of the identical noise component. One can check this by looking at the residuals (i.e. $n_c(t) - n_c(t + \Delta)$) of the identical noise after the subtraction. It is easy to show that the power spectrum of the residual $S_n(f)$ becomes

$$S_n(f) = S_c(f)[1 - \cos(2\pi f\Delta)], \quad (\text{E1})$$

where $S_c(f)$ is the noise spectrum of n_c , Δ is the time difference between the two epochs and is thus roughly the time span of one observing session. The clock noise $S_c(f)$ dominates at low frequencies with time scales of ten years, thus we can check the residual at such frequencies, where the residual power spectrum becomes

$$S_n(f) \simeq \left[1.5 \times 10^{-6} \left(\frac{f}{10 \text{ yr}^{-1}} \right)^2 \left(\frac{\Delta}{1 \text{ day}} \right)^2 \right] S_c(f) \quad (\text{E2})$$

Thus, if we keep each observation session compact within a few days, the clock error can still be significantly (factor of $\sim 10^6$) suppressed by post processing, and we do not need to worry about such common noise for planning an observing schedule at this stage.